Development of new chemical tools to study the cannabinoid receptor type 2

Paus, L.V. de

Chapter 6

Discussion & Future Prospects

Discussion & Future Prospects

The use of *Cannabis sativa* reaches as far back as 2700 B.C. when it's use as a therapeutical drug was discovered by Emperor Sheng Nun[1–5] and later written down in his pharmacopoeia.[1] The *Cannabis* preparations were prescribed a wide array of uses, including for arthritis, enhancement of appetite, depression, inflammation, pain[3], disorders of the female reproductive system, constipation and more.[1] Δ^9-tetrahydrocannabinol (THC) was discovered as the main psychoactive ingredient in *cannabis sativa* in 1942, though it's structure wasn't elucidated until 1964[6]. THC has since been approved for use against chemotherapy-induced nausea[7], enhancement of appetite in AIDS-patients and treatment of symptoms of multiple sclerosis patients[6,8]. CB_1R and CB_2R are the main receptors that bind THC, and over the last several decades research has been devoted to understanding their role in pathologies and developing improved therapeutics for many different diseases. Nonetheless, our understanding of the molecular mode-of-action CBRs is still limited. Information about cellular expression and distribution dynamics; target engagement and the activation mechanism is required to aid in therapeutic development. To this end novel chemical tools are required to investigate these properties of the cannabinoid receptors.

This thesis describes the development of several chemical tools for the study of CB_2R to further understand how the CB_2 receptor accomplices its effect and how selectivity over CB_1R can be retained when designing new ligands (**Chapter 2**-**4**). In the last chapter a new method to avoid the psychoactive effects of CB_1R engagement is proposed by selectively targeting a specific subset of the CB_1 receptors (**Chapter 5**).

The selectivity of ligands

Three-dimensional protein structures may reveal information on the mechanics of the protein, how they malfunction in disease and how to optimally target them with drugs. Despite the advances in modelling software, any *in silico* data generated should be validated with mutational data.[9] Furthermore, design of new therapeutics may benefit from information about the binding mode.

CB_2R agonists are being investigated as therapeutic agents in the clinic. However, their molecular mode-of-action is not fully understood. **Chapter 2** describes the discovery of LEI-102, a CB_2R agonist, used in conjunction with three other CBR ligands (APD371, HU308, and CP-55,940) to investigate the selective CB_2R activation by investigating their binding kinetics, and employing site-directed mutagenesis and cryo-EM studies. During this study it was found that the amino acid $V261^{5.61}$ in CB_2R (CB_2R-$V261^{5.61}$) and its extracellular loop 2 (ECL2) played an important role in selectivity. Furthermore, CB_2R-$F117^{3.36}$ has a role in receptor activation quite unlike the activity suppression role of CB_1R-$F200^{3.36}$. A quadruple mutation in TM1 and TM7 showed that highly lipophilic HU308 and the endocannabinoids, but not the more polar LEI-102, APD371, and CP-55,940, reach the binding pocket through a membrane channel in TM1-TM7.

In **Chapter 2** the molecular origin of signalling bias was not investigated, as the cryoEM structures were obtained in presence of a G protein only. However, it might be the case that different CB_2R agonists lead to different cellular responses depending on their ability to activate β-arrestin and/or G protein pathways.[10] Biased therapeutics that focus on only one of the two pathways may decrease on-target adverse effects. Three-dimensional ligand-receptor models combined with pharmacological data about functional activity could help in determining what drives signalling bias in order to design new drugs with bias in mind. To evaluate the viability of biased therapeutics further research is required. Among others, the bias of existing drugs should be mapped against their therapeutic uses and side effects. For

example, it was found that G protein-biased JWH133 exhibited prolonged analgesic effects in rodent mono-iodoacetate models, while the analgesic efficacy of β-arrestin biased GW833972A was hampered by rapid internalization of the CB_2 receptor.[11] Thus a biased CB_2R agonist with minimal β-arrestin could have potential as a longer-lasting analgesic. More generally, the determined bias of new drugs could help determine the appropriate use and possibly decrease detrimental side effects.

Development of a toolset for the research on the CB_2 receptor

The CB_2R has therapeutic potential for the treatment of inflammatory disorders. Small molecule probes are desirable to study the pharmacodynamics of the CB_2R. Two-step probes do not yet contain a reporter tag. Only after engagement with the target an *in situ* reaction is used to attach a reporter tag. This allows for smaller probes that are less lipophilic, have improved cell-permeability, higher binding affinity and less non-specific binding than ready-use probes. Furthermore, a diverse selection of reporter tags allows use over a wide array of assays. **Chapter 3** describes the structure-based design of several bifunctional probes based on photoaffinity probe LEI-121. While LEI-121 captures the inactive conformation of CB_2R, one of the new probes captures the active conformation of CB_2R upon irradiation with light. They exhibited good CB_2R affinity, selectivity over CB_1R and could successfully label the receptor in a gel-based ABPP assay. Compound **1** (Figure 6.1) was a partial agonist with good potency (pEC_{50} = 8.56 ± 0.56), while compound **2** (Figure 6.1) was the inverse agonist with the highest potency (pEC_{50} = 7.75 ± 0.19). The two different probes revealed different band patterns in gel-based ABPP, capturing the different states of CB_2R.

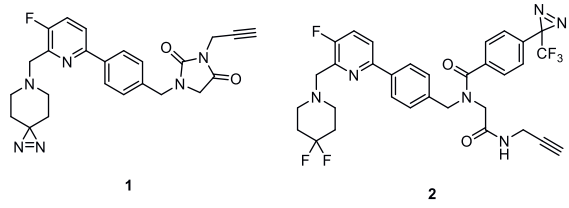

Figure 6.1 The chemical structures of partial CB_2R agonist **1** (nr. **2** in chapter 3) and inverse CB_2R agonist **2** (nr. **3** in chapter 3) from **Chapter 3**.

The covalent probes in **Chapter 3** have a photoreactive that can be activated by UV light. This diminishes off-target activity compared to normal warheads such as Michael acceptors; and the small size of the diazirine minimally affects potency of the compound. The bifunctional, photoreactive probe provides new options for studying proteins, such as with electrophoresis and proteomics.[12] In combination with an alkyne group to introduce different tags to the probe, a multi-purpose probe was created. A fluorophore can be used for visualization, biotin or similar for protein enrichment[13], or even radio-tags for radiopharmacology.[14] The efficacy of the probe should be evaluated over the different applications including electrophoreses, ABPP and flow cytometry, to determine the reach of this new two-step photoaffinity probe.[15]

While two-step probes can be applied over many different applications, they are incompatible with assays that require immediate read-out, or do not tolerate the copper-click conditions required to attach a recognizable tag. One-step probes are particularly useful for live-imaging.[16] Thus a complete toolbox to research CB_2R includes more than one probe to cover a plethora of applications and receptor states of activity. Fluorescent probes enable the detection of CB_2R in relevant cell types and serve as a chemical tool in cellular target engagement studies. In **Chapter 4**, the structure-based design and synthesis of a new CB_2R selective fluorescent probe was reported. Based on the cryo-EM structure of LEI-102 in complex with the CB_2R, 5-fluoropyridin-2-yl-benzyl-imidazolidine-2,4-dione analogues were synthesized in which a variety of linkers and fluorophores were introduced. Molecular pharmacological

characterization showed that probe **3** (Figure 6.2) containing a Cy5-fluorophore with an alkyl-spacer was the most potent probe with a pK_i of 6.2 ± 0.6. It was selective over the CB_1R and behaved as an inverse agonist (EC_{50} 5.3 ± 0.1, E_{max} -63% ± 6). Probe **3** may serve as a chemical tool in target and lead validation studies for the CB_2R, and its capability to selectively image CB_2R *in situ* should be evaluated next.

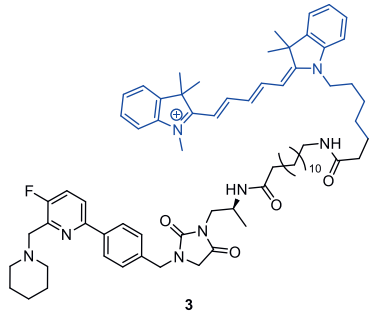

3
pK_i = 6.2 ± 0.6
pEC_{50} = 5.3 ± 0.1

Figure 6.2 The chemical structure of one-step probe **3** (nr. **22** in chapter 4) from **Chapter 4**.

An alternative approach to avoid CB_1R psychoactive effects

Recent developments have shown distinct roles for plasma and mitochondrial CB_1R receptors.[17,18] This could have a profound impact on future therapeutic application of cannabinoids, as several diseases have been linked to dysfunction of just one CB_1R subset.[19,20] For example, congestive heart failure, cardiac ischemic reperfusion injury, diabetes, Alzheimer's and Parkinson's have been linked to dysfunctional mitochondria and changes in OXPHOS respiration.[21] Specific targeting of either plasmalemmal (pl)CB_1R or $mtCB_1R$ may diminish side-effects resulting from activation of the other subgroup. For example, the rewarding feature of Δ^9-THC is a result of disinhibition of dopamine neurons as a result of decreased GABA release.[22] It was recently shown that depolarization-induced suppression of inhibition (DSI) is mediated by $mtCB_1R$, as cell permeable HU210 was able to completely occlude DSI, while HU-biotin only partially occluded DSI.[23] While neither $plCB_1R$ nor $mtCB_1R$ is solely responsible for GABA release inhibition, the rewarding effect on dopamine neurons may be weakened when one subgroup is excluded.

Currently the role of mitochondrial CB_1R ($mtCB_1R$) is determined by comparing effects when inhibiting the CB_1R activity with either a cell- permeable or impermeable antagonist[18], since a $mtCB_1R$ selective agonist is not available. This indirect method relies on absence of activity rather than directly showing effect of activity. A $mtCB_1R$-selective agonist would simplify $mtCB_1R$ role validation by yielding less convoluted results. Additionally, a selective $mtCB_1R$ therapeutic agent could be a possibility to limit undesired side-effects; *i.e.* there would be no $plCB_1R$ activation to dysregulate healthy systems when the pathology only affects $mtCB_1R$ dependent systems. (That is, if such a separation between $plCB_1R$ and $mtCB_1R$ really does exist.) **Chapter 5** described the design and synthesis of several compounds to specifically target $mtCB_1R$. The cationic phosphonium group directs the compound to the negative potential of the mitochondrial membrane.[24,25] CB_1R agonist **4** (Figure 6.3) was designed based on the ORG28611 scaffold with a polyglycerol spacer and tris(4-trifluormethyl)phenyl phosphonium ($TFTPP^+$). Compound **4** showed moderate potency (pEC_{50} = 5.70 ± 0.20) on CB_1R as a partial agonist, and despite affinity for CB_2R did not show significant G protein activity. The $TFTPP^+$ diminished OXPHOS interference compared to TPP^+ while the glycol spacer retained the partial agonist behaviour.

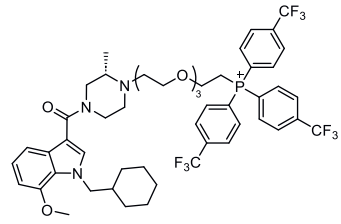

4
pEC_{50} = 5.70 ± 0.20

Figure 6.3 Compound **4** (nr. **4** in chapter 5) from **Chapter 5.**

While compound **4** had moderate activity on CB_1R, it showed a 40-fold decrease in affinity compared to parent structure ORG28611. Adjustments must be made in the structure to diminish the loss of affinity from the $TFTPP^+$ introduction. Only then can the compounds preference for $mtCB_1R$ over $plCB_1R$ be explored. The next step will require an adaptation of previously utilized *in situ* assays. A membrane impermeable antagonist could be used to compete with the agonist compound to determine the origin of its CB_1R activity.[23,26] As an alternative CB_1R activity could be compared in cells with either wild type or mutant DN22-CB_1R (the 22 amino acid deletion limits mitochondrial distribution of the CB_1R).[27] $MtCB_1R$ research is still in its budding stages and much is as of yet unknown.[28–30] However, if future endeavours reveal that there is indeed a distinction between the roles of $plCB_1R$ and $mtCB_1R$, perhaps organelle-specific therapeutics could be a new drug targeting concept.

Manipulating the functional behaviour of ligands

A change in internal efficacy was seen in several chapters after a modification of the parent chemical structure. In **Chapter 3** ring-opening of the imidazolidine in LEI-102 led to a new side chain in the photoaffinity probes that changed efficacy from partial agonist to inverse agonist in a functional [^{35}S]GTPγS assay at CB_2R. Then in **Chapter 4** showed introduction of the lipophilic spacer, but not the hydrophilic polyglycol spacer, changed intrinsic efficacy of the CB_2R partial agonist to inverse agonist. A similar trend was seen with the spacers from the CB_1R agonists in **Chapter 5**, albeit their affinity was low. Despite the large amount of research on the CB receptors, the molecular understanding how ligands assert different intrinsic efficacies is still lacking. In the basic two-state drug receptor interaction model it is assumed there is an equilibrium of the receptor between an active state and quiescent (inactive) state. Agonists stabilize the active state, leading to increased activity, while inverse agonists stabilize the quiescent state and thus decrease activity.[31] However, what interactions make a ligand prefer one state or the other? The recurring observation in **Chapters 3**-**5** is that intrinsic efficacy of a compound can switch by a lipophilic addition. If the newly created protein-ligand interactions can be mapped with for example in cryo-EM structures, perhaps one of the key interactions for (inverse) agonism can be identified. With a molecular understanding of the mechanism for intrinsic efficacy, the design of new ligands could be guided towards a desired functional effect. Additionally, while the type of efficacy is not always relevant for probes, antagonists and inverse agonists have the advantage that they do not affect receptor internalization like agonists do.[10,32,33]

Reducing Off-target Toxicity through Targeted Delivery of Prodrugs

Off-target toxicity and localization are two of the largest bottlenecks in drug discovery. Off-target toxicity may occur when high doses are required to obtain sufficient concentrations at the target location. New research is rekindling a 40 year old idea: High-Density Lipid (HDL) particles can be used to create localized concentration spots.[34] HDL particles occur naturally in the body to transport excess cholesterol to the liver. They are ideal for transport of lipophilic compounds, including drugs, in a stabilizing, biocompatible environment.[35] When an HDL particle arrives at the target destination, it

releases its payload intracellularly by fusing with the plasma membrane. Thereby, an HDL particle can increase a drugs half-life, increase its absorption and facilitate improved targeting depending on lipid composition.[36]

The wide distribution of CB_2R and role in many systems make it both a promising therapeutic target. However, translation to the clinic has proven difficult, with many candidates showing no efficacy. By locally restricting the distribution of ligand the effective concentration of ligand is improved and the therapeutic window is widened by avoiding any potential site that induces side-effects (including off-targets such as CB_1R when not selective enough). For example, CB_2R regulates macrophage differentiation and HDL particles that can specifically target myeloid cells could be useful for drug delivery.[37,38]

Acyloxymethyl Prodrug 5

For this reason the design of LEI-102 was altered to facilitate incorporation of the compound in HDL particles. This requires a lipophilic prodrug that can be incorporated in the lipid formulation of the HDL particle. LEI-102 contains a secondary nitrogen; however, prodrug **5** (Figure 6.4) was designed with a primary alcohol to accommodate a C_{16} alkyl chain in case the secondary nitrogen proved too sterically hindered. With the replacement of isobutyl from LEI-102 with 2-methylpropanol and introduction of the C_{16} alkyl chain the cLogP would increase from 3.3 (LEI-102) to 8.8 (**5**, Chemdraw22). *In vivo* the ester bond should hydrolyse to release compound **10** (Scheme 6.1).

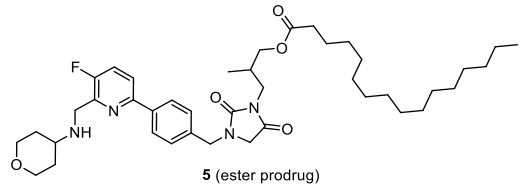

5 (ester prodrug)

Figure 6.4 The Design of the LEI-102-based prodrug **5** where the isobutyl is replaced by 2-methylpropanol to accommodate a C_{16} alkyl chain.

The synthesis of compound **10** (Scheme 6.1) closely followed the synthesis of LEI-102 (Chapter 2). In the first steps 2-methylpropane-1,3-diol was monoprotected with a TBDPS group (**6**) followed by tosylation of the remaining alcohol to give **7**. Next, **7** was coupled with 1-(4-bromobenzyl)imidazolidine-2,4-dione (Chapter 2) to give **8**, which after borylation was directly linked to *N*-((6-bromo-3-fluoropyridin-2-yl)methyl)tetrahydro-2*H*-pyran-4-amine (Chapter 2) to gain **9**. Deprotection with TBAF in the last step led to compound **10** for evaluation of the hydrolysis product.

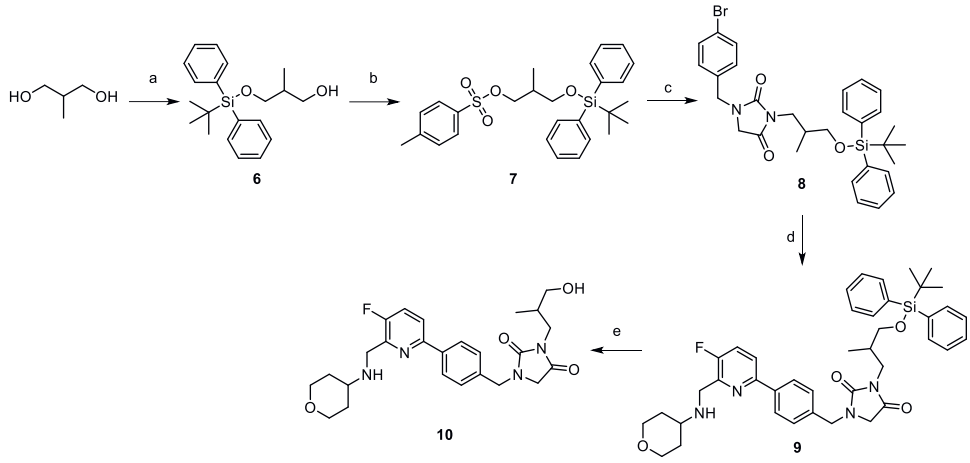

Scheme 6.1 The synthesis of the prodrug precursor. Reagents and conditions: a) *tert*-butylchlorodiphenylsilane, NaH, THF, RT, 24 h, 63%; b) 4-methylbenzenesulfonyl chloride, pyridine, DCM, RT, 144 h, 88%; c) 1-(4-bromobenzyl)imidazolidine-2,4-dione, K_2CO_3, 18-crown-6, DMF, 60 °C, 21 h, 84%; d) i) bis(pinacolato)diboron, Pd(dppf)Cl_2, KOAc, DMF, 75 °C, 23 h, ii) *N*-((6-bromo-3-fluoropyridin-2-yl)methyl)tetrahydro-2*H*-pyran-4-amine, Pd(PPh_3)$_4$, K_2CO_3, toluene:EtOH 4:1 (v/v), 75 °C, 19 h, 34% (two steps); e) TBAF (1 M in THF), RT, 2 h, 23%.

After the synthesis of compound **10**, it was evaluated for affinity (pK_i) on CB_2R in a [^{3}H]CP-55,940 radioligand displacement assay on membranes derived from CHO cells overexpressing hCB_2R_bgal, and compared to the parent compound LEI-102. The results are shown in Figure 6.5B-C.

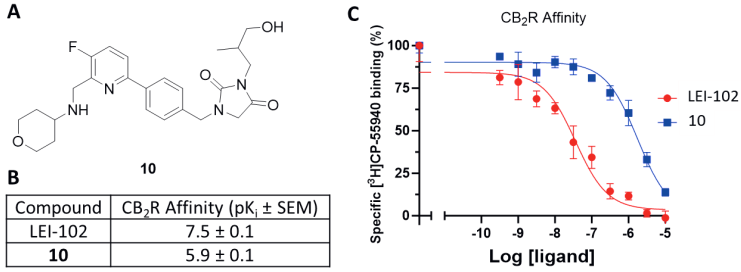

Compound	CB_2R Affinity (pK_i ± SEM)
LEI-102	7.5 ± 0.1
10	5.9 ± 0.1

Figure 6.5 (A) The chemical structure of compound **10**. (B) The affinity (pK_i) of compound **10** compared to LEI-102 determined with a [^{3}H]CP-55,940 radioligand displacement assay on CHO-K1 CB_2R_bgal membranes. (C) Same data displayed as displacement curve data. Binding was normalized to binding of [^{3}H]CP-55,940 at 10 µM. Data are presented as the mean ± SEM from one independent experiment performed in triplicate.

While compound **10** (pK_i 5.9 ± 0.1) shows a decrease in affinity compared to LEI-102, it is still moderately active on CB_2R.

Acyloxyethyloxycarbonyl prodrug 12

As it was observed during synthesis of compound **10** that the secondary nitrogen is sufficiently reactive, an alternative prodrug was designed where a C_{14} alkyl chain was introduced through an acyloxyethyloxycarbonyl (**12**, Scheme 6.2). The resulting prodrug has a high cLogP 9.4 (Chemdraw22) and would hydrolyse *in vivo* to LEI-102.[39] The synthesis of **12** is shown in Scheme 6.2.

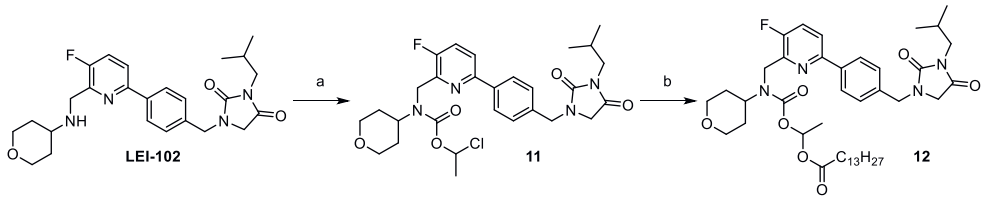

Scheme 6.2 The synthesis of the acyloxyethyloxycarbonyl prodrug of LEI-102 **8**. Reagents and Conditions: a) chloroethylchroloformate, Et_3N, DCM, RT, 2 h, 96%; b) myristic acid, Et_3N, DCM, 100 °C (microwave), 2 h, 30%.

The synthesis of acyloxyethyloxycarbonyl prodrug **12** (Scheme 6.2) started from LEI-102, for which the synthesis is described in **Chapter 2**. Introduction of chloroethyl chloroformate led to **11** in quantitative yield. In the second step myristic acid (C_{14}) was introduced under basic conditions heated in a microwave tube to successfully give prodrug **12**.

With the synthesis complete prodrug **12** has recently been successfully incorporated in HDL particles by Eindhoven university and is currently being tested in murine stroke models to compare the efficacy of HDL-LEI-102 to LEI-102 at Utrecht University (unpublished).

Additionally prodrug **5** synthesis could be completed to compare its performance to prodrug **12**. To finish the synthesis of prodrug **5**, compound **9** should be *N*-bocylated followed by silyl deprotection with TBAF. Acylation of the alcohol can then introduce the lipophilic chain, after which the nitrogen can be deprotected to yield prodrug **5**. After successful synthesis the *in vivo* pharmacodynamics can evaluated.

Final Note

To summarize, this thesis describes the design and synthesis of several new tools that can be used in a wide array of assays to improve our understanding of CB_2R and its function in different systems. It further shows the importance of three-dimensional protein-ligand complexes in understanding selectivity, activity and bias in receptors, and the value of having a receptor-ligand structure in guiding design of new probes and drug candidates. Only when we understand the molecular mode of action of CB_2R, can we learn how to successfully translate *in vitro* activity to clinical efficacy. This could be complemented by an approach to improve pharmacodynamics, such as nanocarriers that improve drug half-life and increase local drug concentration. It is anticipated that the tools presented in this thesis can be used to aid in the endeavour to uncover more about the pharmacological roles of CB_2R and how to successfully develop therapeutic agents targeting CB_2R.

Experimental Section

Chemistry

General Remarks

All reagents and solvents were purchased from commercial sources and were of analytical grade (Sigma-Aldrich, BroadPharm®). Reagents and solvents were not further purified before use. All moisture sensitive reactions were performed under inert atmosphere. Solvents were dried using 4 Å molecular sieves prior to use when anhydrous conditions were required. Water used in reactions was always demineralized. Analytical thin-layer chromatography (TLC) was routinely performed to monitor the progression of a reaction and was conducted on Merck Silica gel 60 F254 plates. Reaction compounds on the TLC plates were visualized by UV irradiation (λ_{254}) and/or spraying with potassium permanganate solution (K_2CO_3 (40 g), $KMnO_4$ (6 g), and H_2O (600 mL)), ninhydrin solution (ninhydrin (1.5 g), *n*-butanol (100 mL) and acetic acid (3.0 mL)) or molybdenum solution ($(NH_4)_6Mo_7O_{24}{\cdot}4H_2O$ (25 g/L) and $(NH_4)_4Ce(SO_4)_4{\cdot}H_2O$ (10 g/L) in sulfuric acid (10%)) followed by heating as appropriate. Purification by

flash column chromatography was performed using Screening Devices B.V. silica gel 60 (40-63 µm, pore diameter of 60 Å). Solutions were concentrated using a Heidolph laborata W8 4000 efficient rotary evaporator with a Laboport vacuum pump. Analytical purity was determined with liquid chromatography-mass spectrometry (LC-MS) using a Finnigan LCQ Advantage MAX apparatus with electrospray ionization (ESI), equipped with a Phenomenex Gemini 3 µm NX-C18 110Å column (50x4.6mm), measuring absorbance at 254 nm using a Waters 2998 PDA UV detector and the m/z ratio by using an Acquity Single Quad (Q1) detector. Injection was with the Finnigan Surveyor Autosampler Plus and pumped through the column with the Finnigan Surveyor LC pump plus to be analysed with the Finnigan Surveyor PDA plus detector. Samples were analysed using eluent gradient 10% → 90% ACN in MilliQ water (+ 0.1% TFA (v/v)). For purification by mass guided preparative high-performance liquid chromatography (Prep-HPLC) the Waters AutoPurification HPLC/MS apparatus was used with a Gemini prep column 5 µm 18C 110 Å (150x21.2mm), Waters 2767 Sample manager, Waters 2545 Binary gradient module, Waters SFO System fluidics organizer, Waters 515 HPLC pump M, Waters 515 HPLC pump L attached to a Waters SQ detector Acquity Ultra performance LC. ^{1}H, ^{13}C, ^{1}H-COSY and HSQC Nuclear Magnetic Resonance (NMR) spectra were recorded on a Bruker AV 300 (300/75 MHz), AV 400 (400/100 MHz) or AV 500 (500/125 MHz) spectrometer at ambient temperature using $CDCl_3$ or DMSO as solvent. Chemical shifts (δ) are referenced in parts per million (ppm) with tetramethylsilane (TMS) or $CDCl_3$ resonance as the internal standard peak ($CDCl_3$/TMS, δ 0.00 for ^{1}H (TMS), δ 77.16 for ^{13}C ($CDCl_3$)). DMSO internal standard peak is ^{1}H: δ 2.50 and ^{13}C: δ 39.52. Multiplicity is reported as s = singlet, d = doublet, dd = doublet of doublet, ddd = doublet of doublet of doublet, dt = doublet of triplet, dq = doublet of quartet, t = triplet, tt = triplet of triplet, q = quartet, p = quintet, hept = heptet, oct = octet, m = multiplet. Coupling-constants (*J*) are reported in Hertz (Hz).

Synthesis of alternative LEI-102 prodrug 5

3-((*tert*-Butyldiphenylsilyl)oxy)-2-methylpropan-1-ol (6): To a cooled (0 °C) and stirred solution of NaH (0.16 g, 60% in mineral oil, 4.0 mmol, 1.2 eq) in anhydrous THF (20 mL) under inert atmosphere was added dropwise 2-methyl-1,3-propanediol (0.3 mL, 3.4 mmol, 1 eq). After 35 minutes TBDPSCl (0.9 mL, 3.5 mmol, 1 eq) was dropwise added at RT. After stirring 24 h at RT the reaction was cooled (0 °C) and quenched with H_2O (20 mL). The layers were separated and the aqueous layer was extracted twice with EtOAc. The combination of organic layers was dried ($MgSO_4$), filtered and the solvent evaporated under reduced pressure. The crude product was purified with flash column chromatography (SiO_2, 10% EtOAc in pentane) to yield a colourless oil (0.70 g, 2.1 mmol, 63%). ^{1}H-NMR (400 MHz, $CDCl_3$) 7.72 – 7.65 (m, 4H), 7.46 – 7.38 (m, 6H), 3.74 (dd, *J* = 10.0, 4.5 Hz, 1H), 3.68 (t, *J* = 5.1 Hz, 2H), 3.60 (dd, *J* = 10.0, 7.7 Hz, 1H), 2.61 (t, *J* = 5.4 Hz, 1H), 2.01 (octet, *J* = 5.8 Hz, 1H), 1.07 (s, 9H), 0.84 (d, *J* = 7.0 Hz, 3H). ^{13}C-NMR (101 MHz, CDCl3) δ 135.72, 135.70, 133.25, 129.93, 127.90, 68.90, 67.84, 37.40, 26.96, 19.27, 13.29.

3-((*tert*-Butyldiphenylsilyl)oxy)-2-methylpropyl 4-methylbenzenesulfonate (7): To a cooled (0 °C) and stirred solution of **2** (0.70 g, 2.1 mmol, 1 eq) in anhydrous DCM (15 mL) under inert atmosphere was added pyridine (1.7 mL, 21.0 mmol, 10 eq) and 4-methylbenzenesulfonyl chloride (0.92 g, 4.8 mmol, 2.3 eq) dissolved in DCM (5 mL). After stirring 144 h at RT the reaction was diluted with NH_4Cl (15 mL) and the layers separated. The aqueous layer was extracted once with DCM. The combination of organic layers was dried ($MgSO_4$), filtered and the solvent evaporated under reduced pressure. The crude product was purified with flash column chromatography (SiO_2, 10% EtOAc in pentane) to yield a colourless oil (0.91 g, 1.9 mmol, 88%). ^{1}H-NMR (500 MHz, $CDCl_3$) δ 7.79 (d, *J* = 8.3 Hz, 2H), 7.59 (dt, *J* = 8.1, 1.7 Hz, 4H), 7.43 (tt, *J* = 7.4, 2.2 Hz, 2H), 7.37 (t, *J* = 7.7 Hz, 4H), 7.31 (d, *J* = 8.0 Hz, 2H), 4.17 – 4.09 (m, 1H), 4.01 (dd, *J* = 9.3, 6.1 Hz, 1H), 3.56 (dd, *J* = 10.2, 4.8 Hz, 1H), 3.47 (dd, *J* = 10.2, 6.6 Hz, 1H), 2.42 (s, 3H), 2.00 (oct, *J* = 6.2 Hz, 1H), 0.98 (s, 9H), 0.89 (d, *J* = 6.9 Hz, 3H).^{13}C-NMR (126 MHz, $CDCl_3$) δ 144.72,

135.64, 135.62, 133.47, 133.44, 133.16, 129.92, 129.82, 128.05, 127.81, 72.23, 64.61, 60.51, 35.75, 26.87, 21.74, 19.32, 14.32, 13.41.

1-(4-Bromobenzyl)-3-(3-((*tert*-butyldiphenylsilyl)oxy)-2-methylpropyl)imidazolidine-2,4-dione (8): A stirred solution of **3** (4.10 g, 8.5 mmol, 2 eq), 1-(4-bromobenzyl)imidazolidine-2,4-dione (1.15 g, 4.3 mmol, 1 eq), K_2CO_3 (3.30 g, 23.9 mmol, 5.6 eq), and 18-crown-6 (0.09 g, 0.3 mmol, 0.1 eq) in anhydrous DMF (80 mL) under inert atmosphere was heated (60 °C) for 21 h. The solution was diluted with brine (80 mL), H_2O (40 mL) and EtOAc (300 mL) and the layers separated. The organic layer was washed twice with brine, dried ($MgSO_4$), filtered and the solvent evaporated under reduced pressure. The crude product was purified with flash column chromatography (SiO_2, 5-15% EtOAc in pentane) to yield a yellow oil (2.09 g, 3.6 mmol, 84%). ^{1}H-NMR (300 MHz, $CDCl_3$) δ 7.68 (tt, *J* = 5.7, 1.7 Hz, 4H), 7.50 – 7.32 (m, 8H), 7.10 (d, *J* = 8.4 Hz, 2H), 4.47 (d, *J* = 2.3 Hz, 2H), 3.65 (dd, *J* = 13.6, 6.7 Hz, 1H), 3.65 (s, 2H), 3.57 (d, *J* = 5.7 Hz, 2H), 3.44 (dd, *J* = 13.6, 8.0 Hz, 1H), 2.24 (oct, *J* = 6.6 Hz, 1H), 1.07 (s, 9H), 0.94 (d, *J* = 6.8 Hz, 3H). ^{13}C-NMR (75 MHz, $CDCl_3$) δ 169.80, 157.06, 135.69, 135.67, 134.64, 133.69, 133.63, 132.22, 129.83, 129.70, 129.67, 127.74, 127.71, 122.24, 66.98, 48.93, 46.13, 42.61, 34.99, 26.92, 19.34, 14.84. LCMS (ESI, 50-90): t_R = 9.91 min; m/z: 579.0 (^{79}Br) + 580.83 (^{81}Br) $[M+H]^+$.

3-(3-((*tert*-Butyldiphenylsilyl)oxy)-2-methylpropyl)-1-(4-(5-fluoro-6-(((tetrahydro-2*H*-pyran-4-yl)amino)methyl)pyridin-2-yl)benzyl)imidazolidine-2,4-dione (9): To a solution of **4** (2.50 g, 4.3 mmol, 1.6 eq) in anhydrous and degassed DMF (75 mL) was added bis(pinacolato)diboron (1.73 g, 6.8 mmol, 2.5 eq), KOAc (1.90 g, 19.4 mmol, 7.2 eq) and a spatula tip Pd(dppf)Cl_2. After heating (75 °C) for 23 h the solution was diluted with H_2O (250 mL) and EtOAc (250 mL) and the layers separated. The aqueous layer was extracted thrice with EtOAc. The combination of organic layers was washed with sat. $NaHCO_3$ (aq), H_2O, and brine, dried ($MgSO_4$), filtered and the solvent evaporated under reduced pressure. To the crude redissolved in toluene:EtOH (75 mL, 4:1, v/v) under inert atmosphere was added *N*-((6-bromo-3-fluoropyridin-2-yl)methyl)tetrahydro-2*H*-pyran-4-amine (0.79 g, 2.7 mmol, 1 eq), K_2CO_3 (2.30 g, 16.6 mmol, 6.2 eq) and a spatula tip $Pd(PPh_3)_4$. After heating (75 °C) for 19 h the mixture was cooled to RT and filtered over a Celite™ pad and diluted with H_2O (120 mL), brine (20 mL), and EtOAc (120 mL). The layers were separated and the aqueous layer was extracted thrice with EtOAc. The combination of organic layers was washed with H_2O and brine, dried ($MgSO_4$), filtered and the solvent evaporated under reduced pressure. The crude product was purified with flash column chromatography (SiO_2, 100% EtOAc) to yield a yellow oil (0.68 g, 0.96 mmol, 36%). ^{1}H-NMR (500 MHz, $CDCl_3$) δ 7.93 (dd, *J* = 8.1, 2.1 Hz, 2H), 7.66 (t, *J* = 7.5 Hz, 4H), 7.60 (d, *J* = 8.6 Hz, 1H), 7.46 – 7.33 (m, 8H), 7.32 (d, *J* = 6.2 Hz, 1H), 4.58 (s, 2H), 4.08 (s, 2H), 4.00 (d, *J* = 11.5 Hz, 2H), 3.69 (s, 2H), 3.65 (dd, *J* = 14.6, 7.6 Hz, 1H), 3.56 (d, *J* = 4.0 Hz, 2H), 3.45 (dd, *J* = 13.4, 8.2 Hz, 1H), 3.39 (t, *J* = 11.5 Hz, 2H), 2.82 – 2.74 (m, 1H), 2.24 (oct, *J* = 6.4 Hz, 1H), 1.90 (d, *J* = 12.1 Hz, 2H), 1.54 (dq, *J* = 10.4, 3.5 Hz, 2H), 1.06 (s, 9H), 0.93 (d, *J* = 4.9 Hz, 3H). ^{13}C-NMR (126 MHz, $CDCl_3$) δ 170.04, 157.17, 156.92 (d, *J* = 256.4 Hz), 152.16 (d, *J* = 4.8 Hz), 147.26 (d, *J* = 16.3 Hz), 138.51, 136.27, 135.76, 135.74, 133.74 (d, *J* = 7.7 Hz), 129.74, 129.71, 128.64, 127.78, 127.76, 127.50, 123.64 (d, *J* = 19.8 Hz), 120.16 (d, *J* = 4.0 Hz), 67.06, 66.83, 53.74, 49.04, 46.49, 45.26, 42.67, 35.07, 33.71, 26.97, 19.40, 14.87.

1-(4-(5-Fluoro-6-(((tetrahydro-2H-pyran-4-yl)amino)methyl)pyridin-2-yl)benzyl)-3-(3-hydroxy-2-methylpropyl)imidazolidine-2,4-dione (10): A solution of **5** (0.20 g, 0.29 mmol, 1 eq) and TBAF (0.34 mL, 1 M in THF, 0.34 mmol, 1.2 eq) in anhydrous THF (10 mL) under inert atmosphere was stirred (RT) for 2 h. The reaction was diluted with H_2O (5 mL) and the aqueous layer was extracted thrice with EtOAc. The combination of organic layers was washed with H_2O and brine, dried ($MgSO_4$), filtered and the solvent evaporated under reduced pressure. The crude product was purified with flash column chromatography (SiO_2, 2-10% MeOH in DCM) to yield a colourless amorphous solid (31 mg, 0.07 mmol, 23%). ^{1}H-NMR (400 MHz, $CDCl_3$) δ 7.94 (d, *J* = 8.3 Hz, 2H), 7.60 (dd, *J* = 8.6, 3.6 Hz, 1H), 7.42 (t, *J* = 8.7

Hz, 1H), 7.33 (d, *J* = 8.3 Hz, 2H), 4.61 (dt, *J* = 15.0, 9.1 Hz, 2H), 4.07 (d, *J* = 2.0 Hz, 2H), 3.98 (ddd, *J* = 11.8, 4.3, 2.4 Hz, 2H), 3.80 (s, 2H), 3.76 – 3.69 (m, 1H), 3.56 (dd, *J* = 6.3, 2.6 Hz, 2H), 3.50 (dd, *J* = 12.0, 4.1 Hz, 1H), 3.44 – 3.30 (m, 3H), 2.78 (tt, *J* = 10.5, 4.1 Hz, 1H), 2.47 (bs, 1H), 2.05 – 1.94 (m, 1H), 1.90 (ddd, *J* = 12.6, 4.3, 2.1 Hz, 2H), 1.54 (ddd, *J* = 23.6, 12.3, 4.4 Hz, 2H), 0.94 (d, *J* = 7.0 Hz, 3H). ^{13}C-NMR (101 MHz, $CDCl_3$) δ 170.66, 157.75, 156.89 (d, *J* = 256.7 Hz), 152.04 (d, *J* = 4.9 Hz), 147.06 (d, *J* = 16.4 Hz), 138.60, 135.91, 128.65, 127.56, 123.67 (d, *J* = 19.7 Hz), 120.20 (d, *J* = 4.1 Hz), 66.79, 64.11, 53.73, 49.16, 46.56, 45.12, 40.99, 35.33, 33.58, 14.73. LCMS (ESI, 10-90): t_R = 4.1 min; m/z: 471.27 $[M+H]^+$. HRMS $[C_{25}H_{31}FN_4O_4]^+$: 471.24021 calculated, 471.24009 found.

Synthesis of LEI-102 prodrug 12**.**

1-Chloroethyl ((3-fluoro-6-(4-((3-isobutyl-2,4-dioxoimidazolidin-1-yl)methyl)phenyl)pyridin-2-yl)methyl)(tetrahydro-2*H*-pyran-4-yl)carbamate (11): To a cooled (°0C) and stirred solution of LEI102 (250 mg, 0.55 mmol, 1 eq) and Et_3N (0.31 mL, 2.20 mmol, 4 eq) in DCM (8 mL) under inert atmosphere (Ar) was added dropwise 1-chloroethyl chloroformate (0.12 mL, 1.10 mmol, 2 eq) in DCM (10 mL). After stirring at 0 °C for 2 h the reaction was quenched with H_2O (20 mL). The layers were separated and the aqueous layer was extracted twice with DCM. The combination of organic layers was dried (Na_2SO_4), filtered, and the solvent evaporated under reduced pressure to yield a brown oil as crude. The crude was used without purification in the next step.

1-((((3-Fluoro-6-(4-((3-isobutyl-2,4-dioxoimidazolidin-1-yl)methyl)phenyl)pyridin-2-yl)methyl)(tetrahydro-2*H*-pyran-4-yl)carbamoyl)oxy)ethyl tetradecanoate (12): A stirred mixture of crude **8** (309 mg, 0.55 mmol, 1 eq), Et_3N (0.31 mL, 2.2 mmol, 4 eq) and myristic acid (503 mg, 2.2 mmol, 4 eq) in DCM (4 mL) in a sealed microwave vial was heated (110 °C) for 2 h in the microwave. The reaction mixture was diluted with H_2O (20 mL) and DCM (20 mL). The layers were separated and the aqueous layer extracted twice with DCM. The combination of organic layers was dried (Na_2SO_4), filtered, and the solvent evaporated under reduced pressure. The crude product was purified with flash column chromatography (SiO_2, 50% acetone/toluene (1:1 v/v) in pentane) to yield a white solid (218 mg, 0.29 mmol, 53%). ^{1}H-NMR (500 MHz, DMSO) δ 8.02 (d, *J* = 8.0 Hz, 2H), 7.93 (d, *J* = 3.4 Hz, 1H), 7.75 (t, *J* = 9.1 Hz, 1H), 7.37 (d, *J* = 8.4 Hz, 2H), 6.62 (d, *J* = 5.4 Hz, 1H), 4.68 – 4.58 (m, 2H), 4.54 (s, 2H), 4.17 (d, *J* = 11.8 Hz, 1H), 3.93 (s, 2H), 3.85 (bs, 2H), 3.32 (s, 2H), 3.22 (d, *J* = 7.3 Hz, 2H), 2.08 – 1.99 (m, 2H), 1.95 (hept, *J* = 6.8 Hz, 1H), 1.82 – 1.67 (m, 2H), 1.64 (t, *J* = 11.8 Hz, 2H), 1.47 (d, *J* = 6.1 Hz, 2H), 1.28 – 1.08 (m, 23H), 0.86 (s, 3H), 0.85 (s, 6H). ^{13}C-NMR (126 MHz, DMSO) δ 170.90, 170.29, 156.82, 154.95, 153.29, 150.84, 145.12, 137.33, 136.87, 127.95, 126.51, 123.96 (d, J = 19.1 Hz), 120.11 – 120.01 (m), 88.73, 66.54, 53.78, 53.46, 49.33, 45.49, 45.48, 42.24, 33.22, 31.26, 30.43, 29.01, 28.98, 28.91, 28.79, 28.68, 28.56, 28.52, 28.12, 26.96, 24.47, 24.03, 22.06, 19.85, 19.34, 13.92. LC-MS (ESI, 10-90): t_R = 15.02 min; m/z = 753.17 $[M+H]^+$. HRMS $[C_{42}H_{61}FN_4O_7 + H]^+$: 753.45970 calculated, 753.45937 found.

Biology

All biologic assays have been previously described. “General remarks”, “Quantification and statistical analysis”, “Cell culture”, “Membrane preparation”, and “[^{3}H]CP-55,940 Heterologous Displacement Assays” can be referenced in **Chapter 2.**

References

1 Zuardi AW. History of cannabis as a medicine: a review. *Rev Bras Psiquiatr*. 2006;28(2):153-157. doi:10.1590/S1516-44462006000200015

2. THC Museum. The History of Cannabis Museum. https://thcmuseum.org/the-history/. Accessed June 1, 2022.

3. The University of Sydney. History of Cannabis. https://www.sydney.edu.au/lambert/medicinal-cannabis/history-of-cannabis.html. Accessed June 1, 2022.

4. Unschuld PU. *Medicine in China: A History of Pharmaceutics*. 1st ed. University of California Press; 1986. https://books.google.nl/books?id=WUgsy0yLEfoC&pg=PA17&lpg=PA17&dq=Pen-ts%27ao+Ching&source=bl&ots=ieyOAa1MV4&sig=ACfU3U2dxbRUqZWdZLVKOom7ZlvwZSv9yQ&hl=nl&sa=X&ved=2ahUKEwi76ZOk44v4AhUVg_0HHYBwA74Q6AF6BAgXEAM#v=onepage&q=Pen-ts'ao Ching&f=false.

5. Adams IB, Martin BR. Cannabis: pharmacology and toxicology in animals and humans. *Addiction*. 1996;91(11):1585-1614. http://www.ncbi.nlm.nih.gov/pubmed/8972919.

6. Pertwee RG. Cannabinoid pharmacology: the first 66 years. *Br J Pharmacol*. 2006;147(S1):S163-S171. doi:10.1038/sj.bjp.0706406

7. Laszlo J, Lucas VS, Hanson DC, Cronin CM, Sallan SE. Levonantradol for chemotherapy-induced emesis: phase I-II oral administration. *J Clin Pharmacol*. 1981;21(S1):51S-56S. doi:10.1002/j.1552-4604.1981.tb02573.x

8. Robson P. Human Studies of Cannabinoids and Medicinal Cannabis. In: *Cannabinoids*. Berlin/Heidelberg: Springer-Verlag; 2005:719-756. doi:10.1007/3-540-26573-2_25

9. Alhumaydhi FA, Aljasir MA, Aljohani ASM, et al. Probing the interaction of memantine, an important Alzheimer's drug, with human serum albumin: In silico and in vitro approach. *J Mol Liq*. 2021;340:116888. doi:10.1016/j.molliq.2021.116888

10. Ibsen MS, Connor M, Glass M. Cannabinoid CB 1 and CB 2 Receptor Signaling and Bias. *Cannabis Cannabinoid Res*. 2017;2(1):48-60. doi:10.1089/can.2016.0037

11. Mlost J, Kostrzewa M, Borczyk M, et al. CB2 agonism controls pain and subchondral bone degeneration induced by mono-iodoacetate: Implications GPCR functional bias and tolerance development. *Biomed Pharmacother*. 2021;136:111283. doi:10.1016/j.biopha.2021.111283

12. Soethoudt M, Stolze SC, Westphal M V., et al. Selective Photoaffinity Probe That Enables Assessment of Cannabinoid CB 2 Receptor Expression and Ligand Engagement in Human Cells. *J Am Chem Soc*. 2018;140(19):6067-6075. doi:10.1021/jacs.7b11281

13. Speers AE, Cravatt BF. Activity-Based Protein Profiling (ABPP) and Click Chemistry (CC)-ABPP by MudPIT Mass Spectrometry. *Curr Protoc Chem Biol*. 2009;1:29-41. doi:10.1002/9780470559277.ch090138

14. Chaturvedi S, Mishra AK. Small Molecule Radiopharmaceuticals – A Review of Current Approaches. *Front Med*. 2016;3. doi:10.3389/fmed.2016.00005

15. Sarott RC, Westphal M V., Pfaff P, et al. Development of High-Specificity Fluorescent Probes to Enable Cannabinoid Type 2 Receptor Studies in Living Cells. *J Am Chem Soc*. 2020;142(40):16953-16964. doi:10.1021/jacs.0c05587

16. Punt JM, van der Vliet D, van der Stelt M. Chemical Probes to Control and Visualize Lipid Metabolism in the Brain. *Acc Chem Res*. 2022;55(22):3205-3217.

doi:10.1021/acs.accounts.2c00521

17. Singlár Z, Ganbat N, Szentesi P, et al. Genetic Manipulation of CB1 Cannabinoid Receptors Reveals a Role in Maintaining Proper Skeletal Muscle Morphology and Function in Mice. *Int J Mol Sci*. 2022;23(24):15653. doi:10.3390/ijms232415653

18. Ma L, Jia J, Niu W, et al. Mitochondrial CB1 receptor is involved in ACEA-induced protective effects on neurons and mitochondrial functions. *Sci Rep*. 2015;5(1):12440. doi:10.1038/srep12440

19. Morales P, Jagerovic N. Novel approaches and current challenges with targeting the endocannabinoidsystem. *Expert Opin Drug Discov*. 2020;15(8):917-930. doi:https://doi.org/10.1080/17460441.2020.1752178

20. Wu Y, Chen M, Jiang J. Mitochondrial dysfunction in neurodegenerative diseases and drug targets via apoptotic signaling. *Mitochondrion*. 2019;49:35-45. doi:10.1016/j.mito.2019.07.003

21. Kulkarni CA, Fink BD, Gibbs BE, et al. A Novel Triphenylphosphonium Carrier to Target Mitochondria without Uncoupling Oxidative Phosphorylation. *J Med Chem*. 2021;64(1):662-676. doi:10.1021/acs.jmedchem.0c01671

22. Friend L, Weed J, Sandoval P, Nufer T, Ostlund I, Edwards JG. CB1-Dependent Long-Term Depression in Ventral Tegmental Area GABA Neurons: A Novel Target for Marijuana. *J Neurosci*. 2017;37(45):10943-10954. doi:10.1523/JNEUROSCI.0190-17.2017

23. Bénard G, Massa F, Puente N, et al. Mitochondrial CB 1 receptors regulate neuronal energy metabolism. *Nat Neurosci*. 2012;15(4):558-564. doi:10.1038/nn.3053

24. Ross MF, Kelso GF, Blaikie FH, et al. Lipophilic triphenylphosphonium cations as tools in mitochondrial bioenergetics and free radical biology. *Biochem*. 2005;70(2):222-230. doi:10.1007/s10541-005-0104-5

25. Murphy MP, Smith RAJ. Targeting Antioxidants to Mitochondria by Conjugation to Lipophilic Cations. *Annu Rev Pharmacol Toxicol*. 2007;47(1):629-656. doi:10.1146/annurev.pharmtox.47.120505.105110

26. Heimann AS, Gomes I, Dale CS, et al. Hemopressin is an inverse agonist of CB 1 cannabinoid receptors. *Proc Natl Acad Sci*. 2007;104(51):20588-20593. doi:10.1073/pnas.0706980105

27. Djeungoue-Petga M-A, Hebert-Chatelain E. Linking Mitochondria and Synaptic Transmission: The CB1 Receptor. *BioEssays*. 2017;39(12):1700126. doi:10.1002/bies.201700126

28. Castaneda JT, Harui A, Roth MD. Regulation of Cell Surface CB2 Receptor during Human B Cell Activation and Differentiation. *J Neuroimmune Pharmacol*. 2017;12(3):544-554. doi:10.1007/s11481-017-9744-7

29. Brailoiu GC, Deliu E, Marcu J, et al. Differential activation of intracellular versus plasmalemmal CB2 Cannabinoid receptors. *Biochemistry*. 2014;53(30):4990-4999. doi:10.1021/bi500632a

30. Schuchman EH, Ledesma MD, Simonaro CM. New paradigms for the treatment of lysosomal storage diseases: targeting the endocannabinoid system as a therapeutic strategy. *Orphanet J Rare Dis*. 2021;16(1):151. doi:10.1186/s13023-021-01779-4

31. Khilnani G, Khilnani A. Inverse agonism and its therapeutic significance. *Indian J Pharmacol*. 2011;43(5):492. doi:10.4103/0253-7613.84947

32. Chen X, Zheng C, Qian J, et al. Involvement of β-arrestin-2 and Clathrin in Agonist-Mediated Internalization of the Human Cannabinoid CB2 Receptor. *Curr Mol Pharmacol*.

2015;7(1):67-80. doi:10.2174/1874467207666140714115824

33. Grimsey NL, Goodfellow CE, Dragunow M, Glass M. Cannabinoid receptor 2 undergoes Rab5-mediated internalization and recycles via a Rab11-dependent pathway. *Biochim Biophys Acta - Mol Cell Res*. 2011;1813(8):1554-1560. doi:10.1016/j.bbamcr.2011.05.010

34. Counsell RE, Pohland RC. Lipoproteins as potential site-specific delivery systems for diagnostic and therapeutic agents. *J Med Chem*. 1982;25(10):1115-1120. doi:10.1021/jm00352a001

35. Lacko AG, Sabnis NA, Nagarajan B, McConathy WJ. HDL as a drug and nucleic acid delivery vehicle. *Front Pharmacol*. 2015;6. doi:10.3389/fphar.2015.00247

36. Zaro JL. Lipid-based drug carriers for prodrugs to enhance drug delivery. *AAPS J*. 2015;17(1):83-92. doi:10.1208/s12248-014-9670-z

37. Javed H, Azimullah S, Haque ME, Ojha SK. Cannabinoid Type 2 (CB2) Receptors Activation Protects against Oxidative Stress and Neuroinflammation Associated Dopaminergic Neurodegeneration in Rotenone Model of Parkinson's Disease. *Front Neurosci*. 2016;10. doi:10.3389/fnins.2016.00321

38. Mulder WJM, van Leent MMT, Lameijer M, Fisher EA, Fayad ZA, Pérez-Medina C. High-Density Lipoprotein Nanobiologics for Precision Medicine. *Acc Chem Res*. 2018;51(1):127-137. doi:10.1021/acs.accounts.7b00339

39. Hilaire JR, Bade AN, Sillman B, et al. Creation of a long-acting rilpivirine prodrug nanoformulation. *J Control Release*. 2019;311-312:201-211. doi:10.1016/j.jconrel.2019.09.001

Acknowledgements

This work was supported by the Dutch Research Council (NWO, Navistroke #15851) (Mario van der Stelt[d], M.v.d.S.).

Author contributions: Conducting Experiments, L.V.d.P. (Laura V. de Paus), R.J.B.H.N.v.d.B (Richard J. B. H. N. van den Berg), J.R. (Joel Rüegger); Writing-Original Draft, L.V.d.P.; Writing Review & Editing, M.v.d.S., L.H.H. (Laura H. Heitman), R.J.B.H.N.v.d.B; Supervision, R.J.B.H.N.v.d.B., M.v.d.S.